Sedimentary Geology 383 (2019) 1–15

Contents lists available at ScienceDirect

Sedimentary Geology

journal homepage: www.elsevier.com/locate/sedgeo

Evaluating iron as a biomarker of rhythmites — An example from the last Paleozoic ice age of Gondwana

F. Callefo [a,*], F. Ricardi-Branco [a], G.A. Hartmann [a], D. Galante [b], F. Rodrigues [c], L. Maldanis [b], E. Yokoyama [d], V.C. Teixeira [b], N. Noffke [e], D.M. Bower [f,g], E.S. Bullock [h], A.H. Braga [c], J.A.H. Coaquira [i], M.A. Fernandes [j]

[a] Instituto de Geociências, Universidade Estadual de Campinas (UNICAMP), 13083-855, Campinas, Brazil
[b] Brazilian Synchrotron Light Laboratory (LNLS), Brazilian Center for Research in Energy and Materials (CNPEM), 13083-970 Campinas, Brazil
[c] Department of Fundamental Chemistry, Institute of Chemistry, University of São Paulo, 05508-000 São Paulo, Brazil
[d] Instituto de Geociências, Universidade de Brasília, 70910-900 Brasília, Brazil
[e] Department of Ocean, Earth and Atmospheric Sciences, Old Dominion University, Norfolk 23529, VA, USA
[f] Department of Astronomy, University of Maryland, College Park, MD 20742, USA
[g] NASA Goddard Space Flight Center, Greenbelt, MD 20771, USA
[h] Geophysical Laboratory, Carnegie Institution of Washington, 5251 Broad Branch Road, NW, Washington, D.C. 20015, USA
[i] Instituto de Física-Universidade de Brasília, 70919-970 Brasília, Brazil
[j] Laboratório de Paleoecologia e Paleoicnologia, Departamento de Ecologia e Biologia Evolutiva, Universidade Federal de São Carlos, 13565-905 São Carlos, Brazil

ARTICLE INFO

Article history:
Received 20 November 2018
Received in revised form 4 February 2019
Accepted 5 February 2019
Available online 10 February 2019

Editor: Dr. J. Knight

Keywords:
Varvite
Biomineral
Ichnofossils
Glacial deposit
Magnetite
Gondwana

ABSTRACT

Microorganisms play a significant role in mineral precipitation, but detecting them in the fossil record is still a challenge. Here we offer an example of how the detection of biological activity in the sedimentary environment can modify a classical depositional model. This study describes the activity of microorganisms in sedimentary structures and the iron mineral formation during the last Paleozoic Ice Age in southwestern Gondwana, recorded by the "Itu rhythmites", Paraná Basin, Brazil. The Itu rhythmites have been considered to be varve-type deposits that present alternating dark laminae (clay/silt-size sediments) and light layers (sand/gravel-size sediments) of varied thickness, forming couplets. Earlier studies focused on abiotic processes of these structures. We applied different techniques and analytical approaches were used, such as synchrotron-based techniques and rock magnetic techniques, in order to test the biogenicity of iron minerals contained in putative microbially-induced sedimentary structures. By detecting biominerals in this rock succession, the depositional model had to be reconsidered, taking into account the biological activity, the limitations on the specific conditions for bacterial growth, and for mineral precipitation. Therefore, we offer a new depositional model that considers the role of microorganisms in formation of these laminae, and this model can be considered for other iron-rich rhythmic deposits in other places of the world. Considering the effects of temperature and other factors in the bacterial productivity, the deposition of the latest couplets in the outcrop occurred in different seasons and by different depositional processes, corroborating with the non-periodicity of 1 year per lithological couplet.

1. Introduction

The Gondwana supercontinent was subjected to the last Paleozoic Ice Age (LPIA) due to its high paleolatitudes during the late Devonian to the early Carboniferous (Caputo et al., 2008). Changes in continent level had great effects on the restructuring of landscape and biota (Montañez and Poulsen, 2013). Recently, microbial activity has been reported in glacial setting related to the LPIA in Gondwana deposits, such as microbially-induced sedimentary structures (MISS) in the Mafra Formation (Netto et al., 2008) and in Rio Grande do Sul Formation (Noll and Netto, 2018), both from the Itararé Group, Paraná Basin, Brazil. MISS are sedimentary structures caused by benthic microorganisms interacting with physical sediment dynamics (Noffke et al., 1996, 2001; Gerdes et al., 2000; Noffke, 2010). MISS are common in clastic aquatic deposits, but their record in glacial deposits is uncertain, especially during the deglaciation period in Gondwana. The role of bacteria in glaciogenic deposits and the paleoenvironmental conditions relating to the growth of microbial mats is also unclear.

In Brazil, the LPIA is recorded by deposits in the Paraná Basin, mainly in the Itararé Group. In São Paulo State there is a well-known record of this glacial period, the "Itu rhythmites" or "Itu varvites" which is considered to be a classic example of a varve-type deposit (dos Santos et al., 1996; Rocha-Campos, 2002). In previous literature, it is believed that this rhythmite formed by the alternation of two sedimentation types: (i) in cold periods, continental ice retained sand and gravel-size

* Corresponding author.
E-mail address: flavia.callefo@lnls.br (F. Callefo).

https://doi.org/10.1016/j.sedgeo.2019.02.002
0037-0738/

sediments while clay and silt-size sediments in suspension in the water are deposited on the bottom of the water body by decantation, and (ii) in warm periods, ice melted and the sediments which were retained during the winter were then deposited (Rocha-Campos, 2002). The Itu rhythmites were thought to have been deposited in a proglacial lake (Rocha-Campos, 2002) along the front of a glacier during the late Paleozoic. The rhythmites are composed of alternating plane-parallel strata: light-colored, sandstone/siltstone layers (deposited during warm periods by the action of dense turbidity currents) and dark colored, siltstone/mudstone layers (deposited during cold periods, when the lake was frozen). The strata are cm- to mm-scale thick, forming lithological couplets that were deposited annually, according to previous studies, such as Rocha-Campos (2002) and Franco et al. (2012).

However, various crinkled sedimentary surfaces similar to MISS are found at the top of the stratigraphic succession of the Itu rhythmites. These structures concur with invertebrate ichnofossils, i.e., *Cruziana* d'Orbigny, 1842 and *Diplichnites* Dawson, 1873 (Fernandes and Carvalho, 2005) and also are rich in iron. Whereas biomineralization processes in fresh sediments are well known (e.g., Lowenstam, 1981; Skinner, 2005; Konhauser and Riding, 2012), the detection of biominerals in the fossil record still remains a challenge. Distinguishing biominerals from inorganic mineral species or from diagenetic products is difficult, but its detection has significant paleoenvironmental implications. Although there are several studies about the deposition of the Itu rhythmites (e.g., dos Santos et al., 1996; Rocha-Campos, 2002; Caetano-Chang and Ferreira, 2006; Franco et al., 2012), there is still controversy regarding the origin, the paleoenvironment and the periodicity recorded in the vertical extension of the outcrop. Biological precipitation has not been considered.

Here we investigate the occurrence of MISS structures in the Itu rhythmites by combining a multi-method approach, such as petrological, synchrotron-based techniques and rock magnetism analyses, in order to test the biogenicity of these structures, using iron minerals as the main target. If the biological precipitation of minerals played a role, the current paleoenvironmental interpretation and depositional model should potentially incorporated this mechanism. We present an alternative interpretation, considering that the biological precipitation in the rhythmite deposition significantly influenced the depositional dynamics and the paleoecology of bottom dwellers.

2. Study area and geological setting

The Paraná Basin is an intracratonic basin that encompasses approximately 1.7×10^6 km^2 of central-eastern South America. Six supersequences are recognized in this basin: the Rio Ivaí (Ordovician/Silurian), the Paraná (Devonian), the Gondwana I (Carboniferous/Permian), the Gondwana II (Triassic), the Gondwana III (Jurassic/Cretaceous), and the Bauru (Cretaceous). The Gondwana I Super-sequence represents a transgressive-regressive cycle related to variations in sea level during the basin's evolution (Milani et al., 2007). In this unit, the Tubarão and Passa Dois Supergroups occur. The Itu rhythmites belong to the upper part of the Tubarão Supergroup, specifically to the Itararé Group, late Carboniferous (Cagliari et al., 2016). The Itu rhythmites are located in the central-eastern region of São Paulo State, approximately 90 km from São Paulo (Fig. 1).

Following palynological analyses, the Itu rhythmite was deposited during the late Pennsylvanian (Kasimovian/Gzhelian) age, within the *Crucisaccites monoletus* Interval Zone (Souza et al., 2010). According to Caetano-Chang and Ferreira (2006), the light layers have grain sizes of silt to sand, and are composed mainly of quartz grains cemented by calcite and silica, with rare feldspar and mica. The authors also described plane-parallel laminations, bioturbations and dropstones. Dark laminae are interpreted as shales (dos Santos et al., 1996; Caetano-Chang and Ferreira, 2006).

The Itararé Group records the LPIA of the Gondwana Supercontinent (dos Santos et al., 1996). Its marine and continental sediments were deposited under glacial and periglacial climates (Souza et al., 2010). Glacially-controlled deposition in the Paraná Basin started in the Bashkirian (early Pennsylvanian, Carboniferous), when ice moved into the basin interior, reaching up to 200 km inland. According, dos Santos et al. (1996), during deposition of Itu rhythmites, the paleoenvironment consisted of a proglacial lake influenced by the ice streams of the Windhoek Ice Sheet. The last deposits of Itararé Group, as well as the overlying Guatá Group, record a change from the glacial period (LPIA) to the warm period of Cisuralian (Vesely and Assine, 2006).

3. Material and methods

3.1. Samples

Samples were collected close to the "Parque do Varvito" (Varvito Park), in the Ituana quarry (23°16′6.20″ S and 47°19′15.19″ W), next to the urban area of Itu city (Fig. 1). The exposure of rhythmites is around of 10 m high, and the samples for this study were collected in the upper 3 m of the outcrop.

We sampled 32 lithological couplets (dark laminae and light layers) in this study. Two representative samples were chosen for the compositional and magnetic analyzes (Table 1). The collected samples varied in size, ranging from 10 cm^2 to approximately 80 cm^2 in area. The samples were cut to smaller sizes according to the need of each analytical technique applied. All samples are deposited in the Laboratory of Paleoecology and Paleoichnology (LPP) of the Federal University of São Carlos (Brazil).

3.2. Thin section analysis

Oriented thin sections of 2×5 cm size and 30 μm thickness were prepared (without a glass coverslip to allow compositional analyses). Quantitative analysis was made using the point counting from Grazzi-Dickinson method (Dickinson, 1970). The thin sections were analyzed at the Laboratório de Paleohidrogeologia of State University of Campinas (UNICAMP), with a Carl Zeiss petrographic microscope Scope A1 ZEISS. The images were recorded with a ZEISS AxioCam camera and processed with ZEISS AxioVision® 4.8.2.0. (2006) software.

3.3. Material extraction

The sample preparation for scanning electron microscopy (SEM), transmission electron microscopy (TEM) and the rock magnetic analysis was performed at the Brazilian Synchrotron Light Laboratory (LNLS/CNPEM), using the LQI (Chemistry Laboratory) infrastructure. The process started with the milling of dark laminae, following by dissolution with ethanoic acid and sodium acetate. The ferromagnetic material was precipitated and extracted with a neodymium magnet. The extracted material was dried and weighed (following the protocol of Strehlau et al., 2014).

3.4. Electron Microprobe Analysis (EPMA), Scanning Electron Microscopy and Energy Dispersive Spectroscopy (SEM/EDS)

Compositional analysis, elemental maps and images of the samples were acquired with the SEM-FEG ENV (FEI Quanta) equipment at the Brazilian Nanotechnology National Laboratory (LNNano/CNPEM). Secondary electron images were obtained using the Everhart Thornley detector, at an accelerating voltage of 15 to 20 kV. The maps were performed using an Oxford Instruments EDS detector, operating the AZtec software. The nominal resolution of the instrument was 1.8 nm. Additional images, quantitative data and cathodoluminescent (CL) images were collected using the JEOL 8530F electron probe at the Carnegie Institution for Science (Washington, DC). The probe was operated at 15 kV and 20 nA. Elemental maps with a spatial resolution of 1–2 μm were obtained using both WDS detectors and the Thermo Scientific

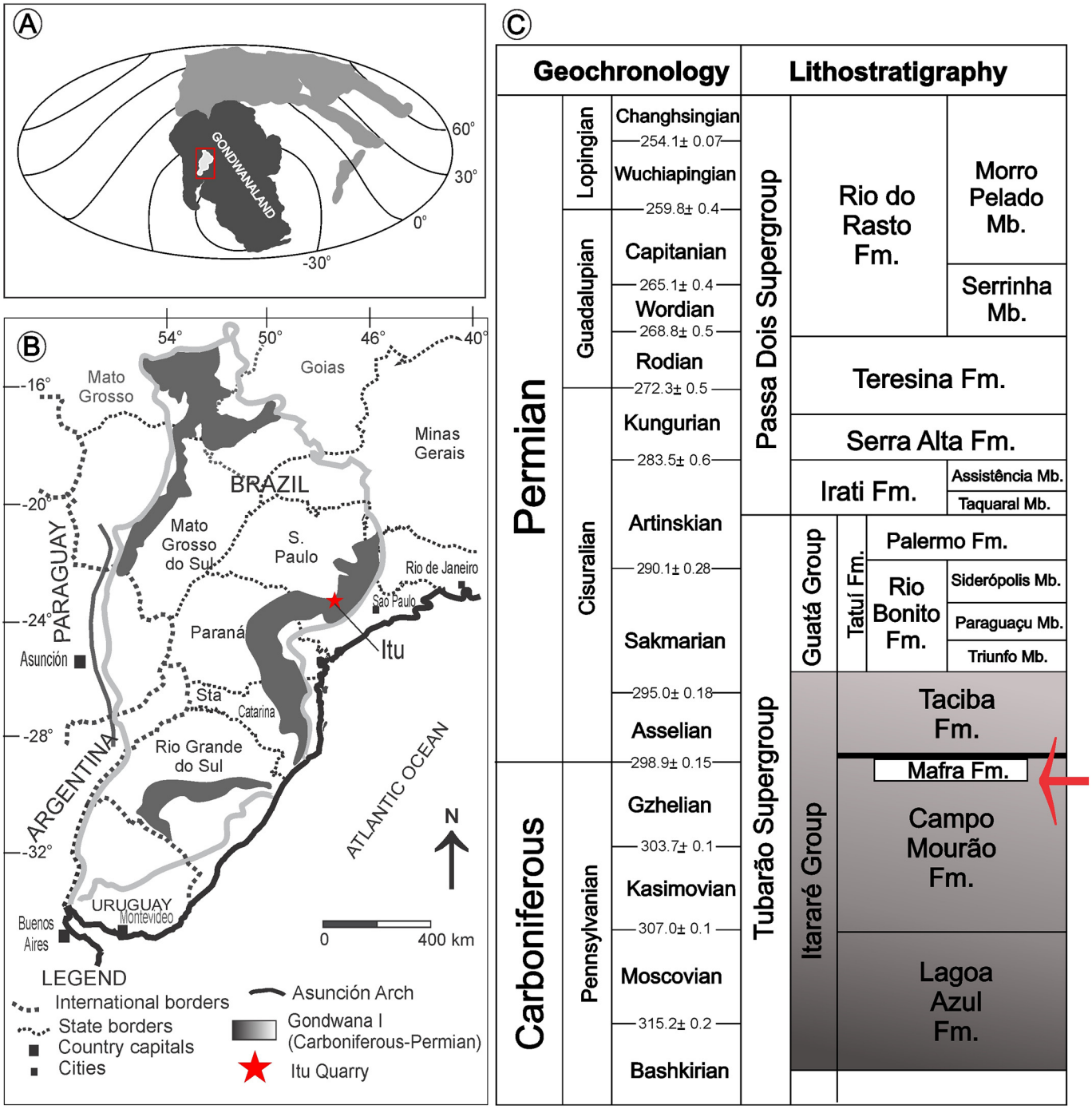

Fig. 1. (A) Paraná Basin (red) in the Gondwana supercontinent in the Lower Permian-Upper Carboniferous, ~360–270 Ma (modified from Veevers, 2004); (B) Paraná Basin with the location of the Itu quarry, showing the Itu rhythmites, red star (modified from Milani et al., 1998); (C) stratigraphic column of the Carboniferous-Permian interval, with the time period of the Mafra Formation, Campo Mourão Formation, Itararé Group (modified from Ianuzzi, 2010). (For interpretation of the references to colour in this figure legend, the reader is referred to the web version of this article.)

Table 1
Samples collected from the Ituana quarry, analysis and techniques applied to each of them.

Sample (total = 32)	Macroscopic analysis	Thin section	SEM/EDS TEM	EPMA	μ-XRF	Magnetic analysis	Raman spectroscopy	XRD
LPP-0042 to 0072	x							
LPP-0041	x	x	x		x	x	x	
LPP-0040	x	x	x	x	x	x		x
LPP-0041 (extract)			x					
LPP-0040 (extract)			x			x		

Noran System 7 EDS system (NSS). Hyperspectral CL images were collected simultaneously using the Ocean Optics xCLent CL system. Individual quantitative analyses were also performed using the NSS system. Samples were coated in iridium to facilitate mapping and analysis of carbon.

3.5. μ-X-ray fluorescence (μ-XRF)

μ-XRF analysis was performed using the XRF beamline at the LNLS/CNPEM. The samples were cut in 4 × 2 cm sized blocks and polished. The beamline was used in micro-beam mode with the KB focusing system in order to reach a beam size of 12 × 25 μm diameter (maximum resolution), at room temperature. The excitation was made in white-beam mode (3–14 keV). The elemental maps were obtained using the PyMca 4.6.0 software (developed by European Synchrotron Radiation Facility - ESRF; Solé et al., 2007).

3.6. Transmission Electron Microscopy (TEM)

The images were obtained using the JEOL JEM 2100F equipment at the Brazilian Nanotechnology National Laboratory (LNNano/CNPEM), with a field-emission gun and acceleration voltage of 200 kV. The extracted magnetic material was allocated in a carbon coated copper grid. The images were obtained in TEM mode, with 4 k × 4 k pixel CCD detector (Gatan). Images were acquired by Digital Michograph software (Gatan). The lattice resolution of the equipment is 1.4 Å.

3.7. Raman Spectroscopy

Raman imaging was performed with a WITec Scanning Near-Field Optical Microscope that has been customized to incorporate confocal Raman spectroscopy imaging. The excitation source was a frequency-doubled solid-state YAG laser (532 nm) operating between 0.01 and 5 mW output power as measured at the sample using a power meter. Optical microscopy images were captured by a camera system attached to the microscope. Objective lenses that were used included a 20× long working distance for large area scans and a 100× oil immersion lens for small area scans, with a 25 μm optical fiber acting as the confocal pinhole. The lateral resolution was as small as 270 nm when using the 100× lens and 810 nm when using the 20× lens. Spectra were collected on a Peltier-cooled Marconi 40–11 CCD chip, after passing through a f/4300 mm focal length imaging spectrometer using a 600 lines/mm grating. The spectral range covered 0 to 4000 cm^{-1}, with a spectral resolution better than 7 cm^{-1}. The instrument produced Raman images by accumulating a Raman spectrum at each image pixel as the sample stage translates. Average spectra were produced using integration times of 1 to 3 s per accumulation and 10 accumulations. Raman peaks of interest were then chosen to create peak intensity maps, and their occurrence throughout the image computed by using a Gaussian fit to the data using WITec Project Plus software. For example, to map the occurrence of the mineral anatase (TiO_2) in the sample, spectra for individual anatase peaks at 143, 399, 513, or 639 cm^{-1} were selected and mapped. After compilation, each spectral map was checked for consistency in peak mapping to ensure the exclusion of interfering peaks or fluorescence background, thus eliminating the possibility of error due to the misidentification of peaks.

3.8. X-ray diffraction

X-ray diffraction analysis was performed using the XRD2 beamline at the LNLS/CNPEM (Giles et al., 2003). The data were obtained with excitation energy of 7 keV, with beam size in order of ~0.5 mm × 1.5 mm (V × H) in resolution of 2θ and 0.003^0. The energy was chosen to be bellow Fe K-edge, thus avoiding the spurious signal from the Fe X-ray fluorescence. The grazing incidence geometry was used to limit the depth of penetration into the sample, to isolate the signal from superficial laminae. The linear Mythen (Detrics) detector, 1 k, was utilized to collect the diffraction data. The samples were cut into small blocks 1 to 2 cm^2 in size and positioned on the goniometer without further manipulation. The analyses were performed in both the dark laminae and light layers.

3.9. Rock magnetism

Rock magnetism measurements were performed at the Laboratório de Paleomagnetismo of University of São Paulo (USPMag) and University of Brasília, Brazil. Acquisition of isothermal remanent magnetization curves (IRM), hysteresis loops, first order reversal curves (FORC) and low-temperature magnetization measurements were performed to determine the magnetic properties of the studied bulk sample and a sample from extracted magnetic material. Hysteresis loops, IRM acquisition curves and FORC diagrams were determined at room temperature. Measurements were performed with applying fields of up to 1 T using a Princeton Measurements Corporation Micromag vibrating sample magnetometer (VSM). Saturation magnetization (Ms), saturation remanent magnetization (Mrs), coercivity (Bc), and coercivity of remanence (Bcr) are all determined from hysteresis and backfield measurements. However, these standard hysteresis parameters provide only a measure of the bulk magnetic properties and therefore are not suitable for discriminating the different magnetic components contributing to the magnetization in samples with mixed or more complex magnetic assemblage. Given the complex magnetic mineralogy in our samples, we used FORC diagrams to identify and discriminate the different magnetic mineral grains (Roberts et al., 2014). FORC measurements were performed at room temperature after 586 reversal curves with an averaging time of 200 ms. FORC diagrams were calculated using the FORCinel software package (Harrison and Feinberg, 2008) using a smoothing factor of 15 for all samples. In addition, low-temperature magnetization measurements were carried out using a Magnetic Property Measurement System XL (Quantum Design) at the University of Brasilia. These measurements were performed in order to identify the transition phases between different magnetic fractions, in particular the Verwey (~120 K) and the Morin (~260 K) transitions for stoichiometric magnetite and hematite, respectively. Measurements of Room Temperature Saturation of IRM (RTSIRM) and Field-Cooling, Zero-Field Cooling (FC/ZFC) curves were carried out on representative sample. Samples were cooled to 10 K in both zero field and 5 T, respectively. At 10 K, a 5 T field was applied and was then switched off to import a RTSIRM and the MPMS was reset. FC/ZFC curves were measured during warming in zero field in scan mode at 5 K/min.

4. Results and interpretations

4.1. Field data

The quarry of Itu rhythmites presents alternating dark and light layers forming couplets. These couplets can reach an average thickness of 45 cm at the bottom of the succession; they thin upward to only 1 to 2 mm at the top. The light layers are in average 50% to 80% thicker than the dark ones; only towards the top of the succession the light and dark laminae present similar thicknesses.

At the top of the succession, low profile ripple marks, as well as wrinkle structures and sinoidal cracks occur on bedding surfaces (Fig. 2). In vertical section, dark laminae become visible. The ripple marks show crest-to-crest distances of 1.5 cm, but have a height of up to 2 mm; the wrinkle structures cover 9 to 108 cm^2 areas and show mm-scale, irregular crinkles of no preferred orientation. The cracks have 15 to 20 mm long and are weathered to a depth of <1 to 2 mm. Ichnofossils are associated with these marks, commonly preserved as positive epirelief. The tracks range from 3 to 10 mm long, and have sometimes a slight sinuosity. They remain surface-parallel and there are no podial

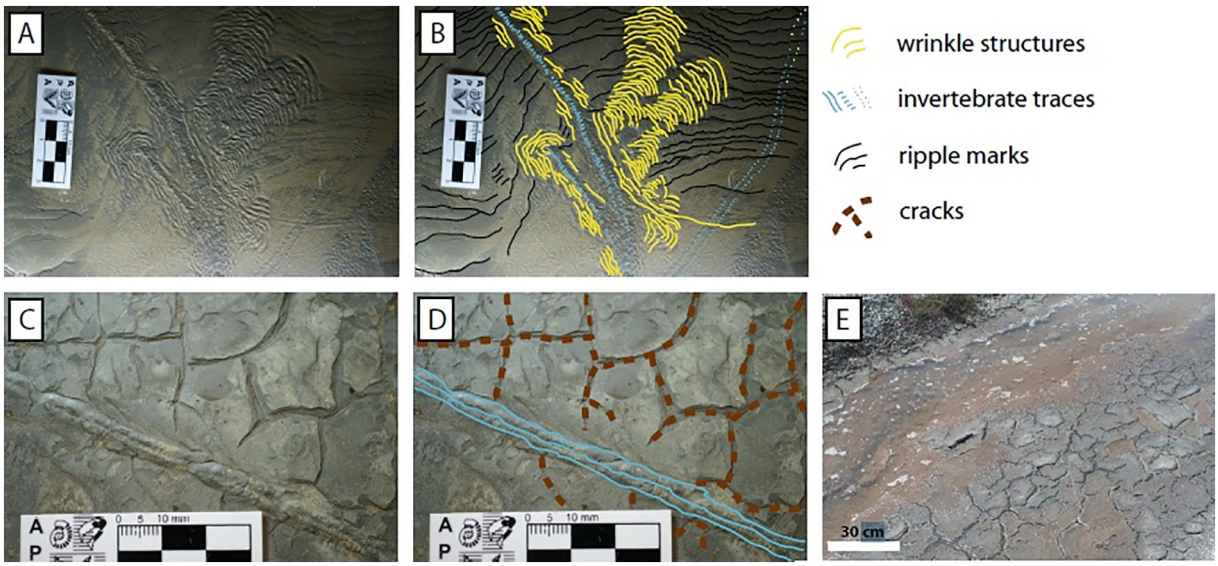

Fig. 2. MISS from the Itu rhythmites: (A) wrinkle structure caused by the invertebrate movements disturbing the coherent microbial mat. Proceeding ripple marks were completely smoothened by the microbial mat. (B) sketch for illustration. (C, D) cracks caused by contraction and rupture of the microbial mats during episodic subaerial exposition. (E) modern microbial mat from LagoaVermelha (Rio de Janeiro, Brazil), showing cracks comparable to the studied samples from Itu rhythmites.

imprints. Fig. 3A shows a vertical section of a couplet, showing a gas dome between the dark laminae.

We interpret the wrinkle structures, the low-profile ripple marks and sinoidal cracks as in situ preserved microbial mats forming MISS. The wrinkle structures were caused by the mechanical stress of invertebrate movement 'bulldozing' through the coherent microbial mat (Fig. 2A, B). The ancient microbial mat was thick enough to cover the proceeding ripple marks like a cloth, so the sediment surface became

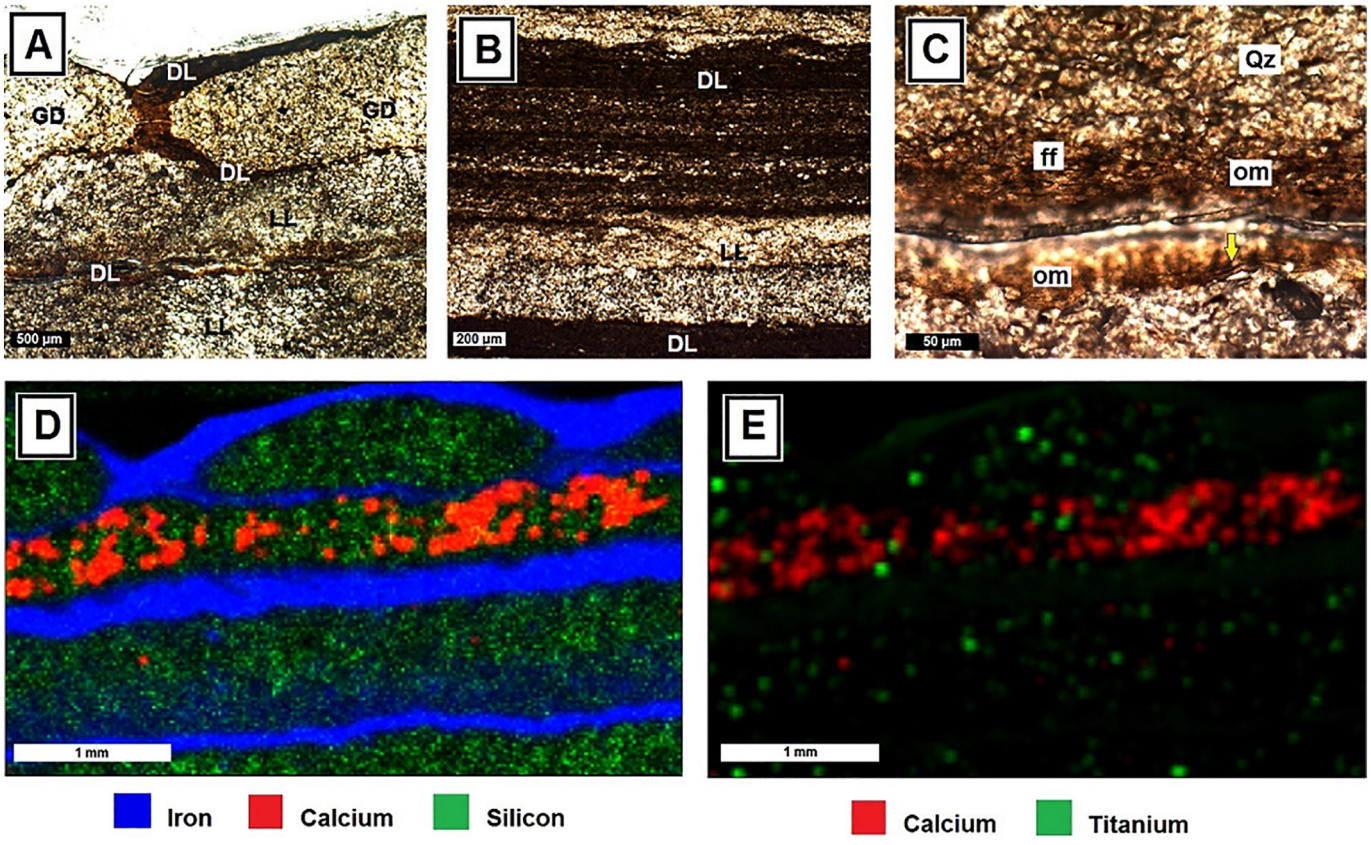

Fig. 3. (A) thin section (sample LPP-0040) showing the dark laminae (DL) and light layers (LL) and the gas domes (GD) filled by silica cement between the dark laminae; (B) thin section (sample LPP-0041) showing the undulating laminations in the top-most layers (towards to the top bed surface) and the intercalation between the dark laminae (DL) and light layers (LL); (C) thin section (sample LPP-0040) showing the difference in the grain size in the dark laminae (DL) and the light layers (LL), quartz grains as the major component in the LL and organic matter (om) in the DL, laminoid-fenestral fabrics (ff) and sinoidal structures (yellow arrow) in the DL; (D) µ-XRF image with elemental map showing the distribution of Fe in the dark laminae and the Ca and Si in the light layers; (E) µ-XRF elemental map with the Ti distributed mainly in the dark laminae, and the Ca in the light layers. (For interpretation of the references to colour in this figure legend, the reader is referred to the web version of this article.)

almost planar. Sinoidal cracks record the episodic desiccation of microbial mats (Fig. 2C, D), a feature also observed in modern microbial mats (Fig. 2E). The domal structure in Fig. 3A is interpreted as a gas dome, developed beneath a sediment-sealing microbial mat, considering the microscope evidence, such as the laminoid-fenestral fabrics associated with the dark laminae (Fig. 3B, C).

The ancient microbial mats developed on the bottom of the water body, and were episodically subaerially exposed along the shore lines, evidenced by the sinoidal cracks (Fig. 2C, D) and the presence of myriapod trace fossils, invertebrates which present tracheal breathing (Ruppert and Barnes, 2004). The substrate was ideal for the proliferation of foraging invertebrates, evidenced by the abundance of ichnofossils attributed to the arthropods myriapods *Isopodichnus* (Bornemann, 1889) and *Diplichnites* (Dawson, 1873).

4.2. Petrology

In vertical section through the MISS, the alternating dark and light layers reveal differences in grain sizes (light layers have grains of silt/sand size whereas dark laminae have grains of mud/silt size). The dark laminae include copious amounts of amorphous organic matter (kerogen) and iron oxide (95 ± 1.73%). Oriented quartz grains in the dark layers make 5 ± 0.81% of the matrix. The light layers consist of 97 ± 2.94% silt and 3 ± 2.64% mud, while the dark laminae consist of 92 ± 1% mud and 8 ± 1.29% silt. Some laminations include silica cement. The main mineral in theses layers is quartz (80 ± 3.55%), in addition to rare feldspar (4 ± 1.29%). Also, iron oxide coating occur (5 ± 1.29%). Biogenic elements, such as palynomorphs, represent a small percentage (1 ± 0.81%). Table 2 shows the quantitative data for dark laminae and light layers.

The vertical sections also reveal that the dark laminae form different MISS including gas domes, fenestrae fabrics, and sinoidal structures. The mm-scale cavities beneath the fossil gas domes are partially or completely filled by silica cement (Fig. 3A). Undulated laminations are present, mainly towards to the bedding surface (Fig. 3B). Fenestral fabrics, characterized by elongated fenestrae pores ranging from in size 20 μm to 50 μm occur in the light-colored layers (Fig. 3C). Gas domes and fenestral fabrics commonly occur together in areas covered by microbial mats: gas domes are local small domes that rise on the depositional surface due to increasing gas pressure beneath a sediment-sealing microbial mat. The gases are also responsible for the formation of the pores, which are aligned parallel to the microbial mat layers. Some of the dark laminae form sinoidal structures of 2 to 5 mm high (Fig. 3C). Sinoidal structures represent ripple marks that were overgrown by microbial mat and then buried. The high concentration of organic matter in the dark layers that build up the various MISS strongly supports the biological interpretation. In contrast, no MISS was detected in the white layers, which probably were formed without any microbial influence.

Table 2
Quantitative petrology of two thin sections, both containing dark laminae and light layers, showing the average value in percentage of the main components for each lamination. The standard deviation (SD) was calculated based in the number of samples = 2. The thin sections analyzed were from the samples LL-0040 and LL-0041.

	Dark laminae		Light layers	
	%	SD	%	SD
Component				
Kerogen/iron	95	1.73	5	1.29
Quartz	5	0.81	80	3.55
Silica cement	0	–	10	2.94
Feldspar	0	–	4	1.29
Pollen	0	–	1	0.81
Grain size				
Mud	92	1.00	3	2.64
Silt	8	1.29	97	2.94

4.3. μ-X-ray fluorescence

Qualitative μ-XRF (X-ray Fluorescence) maps of elemental distributions were acquired from the near surface areas of the samples. The maps showed that iron (Fe) is concentrated in the MISS-forming dark layers, whereas silicon (Si) and other elements that can be attributed to siliciclastic material are distributed in the light layers (Fig. 3D). Titanium (Ti) is distributed throughout the entire samples, but has a slightly higher concentration in the dark laminae (Fig. 3E). Calcium (Ca) is concentrated only in the light layers.

4.4. SEM/EDS and TEM analysis

In SEM/EDS analyses, phyllosilicates (including Si, Al and K) were detected in both the light layers and the dark laminae. In the dark laminae, the quartz and feldspar grains show a smooth surface because it was covered by fossilized bacterial EPS (extracellular polymeric substance). The microtexture was interpreted as a fossil biofilm (Fig. 4A). Magnetic material extracted from the putative biofilm was analyzed by EDS and showed enhanced concentration of Fe (67 to 80%) and oxygen (O) (23 to 26%). Minor percentages of C, Al, Si and Ti also occur (Fig. 4B). In energy dispersive X-ray spectroscopy (EDS), C and O were the main constituents of these putative biofilms (Fig. 4C). Transmission electron microscopy (TEM) images of the putative biofilm suggests elongated hexaoctahedral magnetite nanoparticles 200 to 250 nm of long (Fig. 4D). The extracted material suggests spheroidal nanoparticles of iron minerals (most likely magnetite, according to magnetic analyses, see below) at approximately 30 nm diameter, some of them with octahedral habit (Fig. 4E).

We interpret the data obtained from the dark laminae as indicative for fossil biofilms. The biofilm fossils and the iron composition of the magnetic material extracted from these biofilms supports a bioprecipitation of the iron-bearing minerals. The TEM images suggest iron deposition by magnetotactic bacteria (MTB), although the magnetosome chains were not observed in the SEM images.

4.5. Raman spectroscopy

Raman spectroscopy (Fig. 5) revealed spectral peaks corresponding to anatase (TiO_2) at 143, 399, 513 and 639 cm^{-1}. Quartz (201, 263 and 467 cm^{-1}) and feldspar (sanidine, at 154, 284, 476 and 512 cm^{-1}) were detected. The Raman map of a selected area in the sample LPP-0041 showed that the quartz and feldspar are distributed in both dark and light layers. Although the anatase is distributed in both dark and light layers, it occurs in a higher concentration in the dark ones. Anatase and carbon (peaks at 1351 and 1589 cm^{-1}) are distributed in alignment with the biofilm detected in these laminae, as well the iron detected in the μ-XRF and SEM/EDS analysis.

4.6. X-ray diffraction

The X-ray diffraction analyses were performed on the polished surface of a small block of sample (IcI-009), both in the dark laminae and in the light layers (Fig. 6A). In the dark laminae, the following minerals were detected: muscovite, calcium phosphate, rutile and anatase (Fig. 6B). The most intense anatase Bragg reflection (2θ at 29.26°) appears convoluted with the most intense peak of calcium phosphate ($Ca(PO_3)_2$) (28.99°), which hinders a definitive identification. However, the second most intense peak of the anatase phase, which appears around 55.96°, is evidence that this phase of this mineral is present in the material. Together, this evidence plus the Raman data strongly suggest the presence of anatase in the dark laminae. In the light layers it was possible to acquire the diffractogram of SiO, in the form of α-quartz, as expected (Fig. 6C). The reference code and other standards specifications are shown in Table 3.

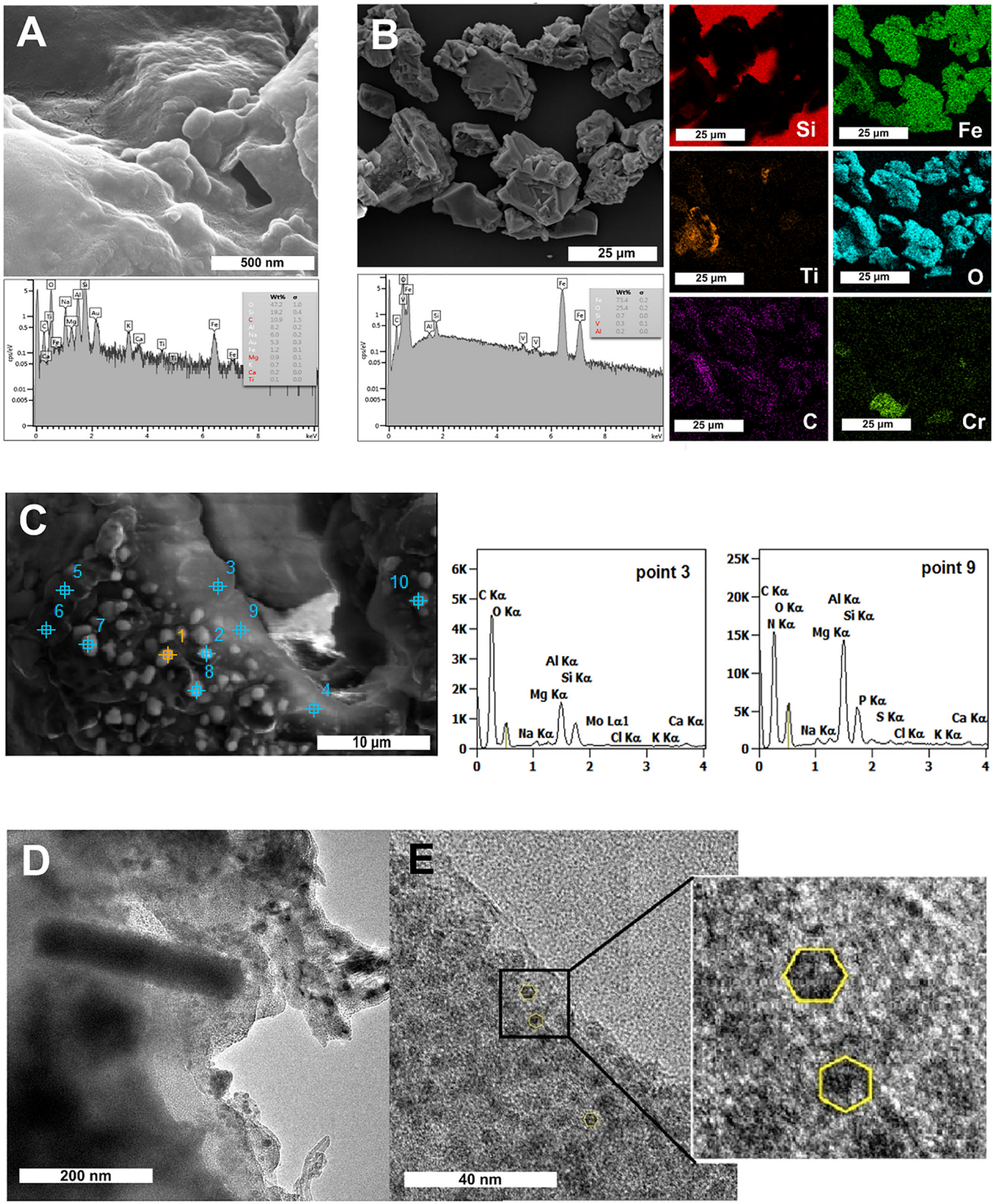

Fig. 4. (A) SEM/EDS analysis in the surface of dark layer showing grains possibly covered by fossil biofilm including EPS; (B) SEM/EDS analysis in the extracted magnetic material and elemental map showing that the main composition is Fe and O, with some minor Cr, Ti and C; (C) grains covered by a smooth texture with a composition compatible to that of modern EPS; (D) putative elongated magnetite crystal related to magnetosome from magnetotactic bacteria; (E) hexoctahedral nanocrystals of magnetite.

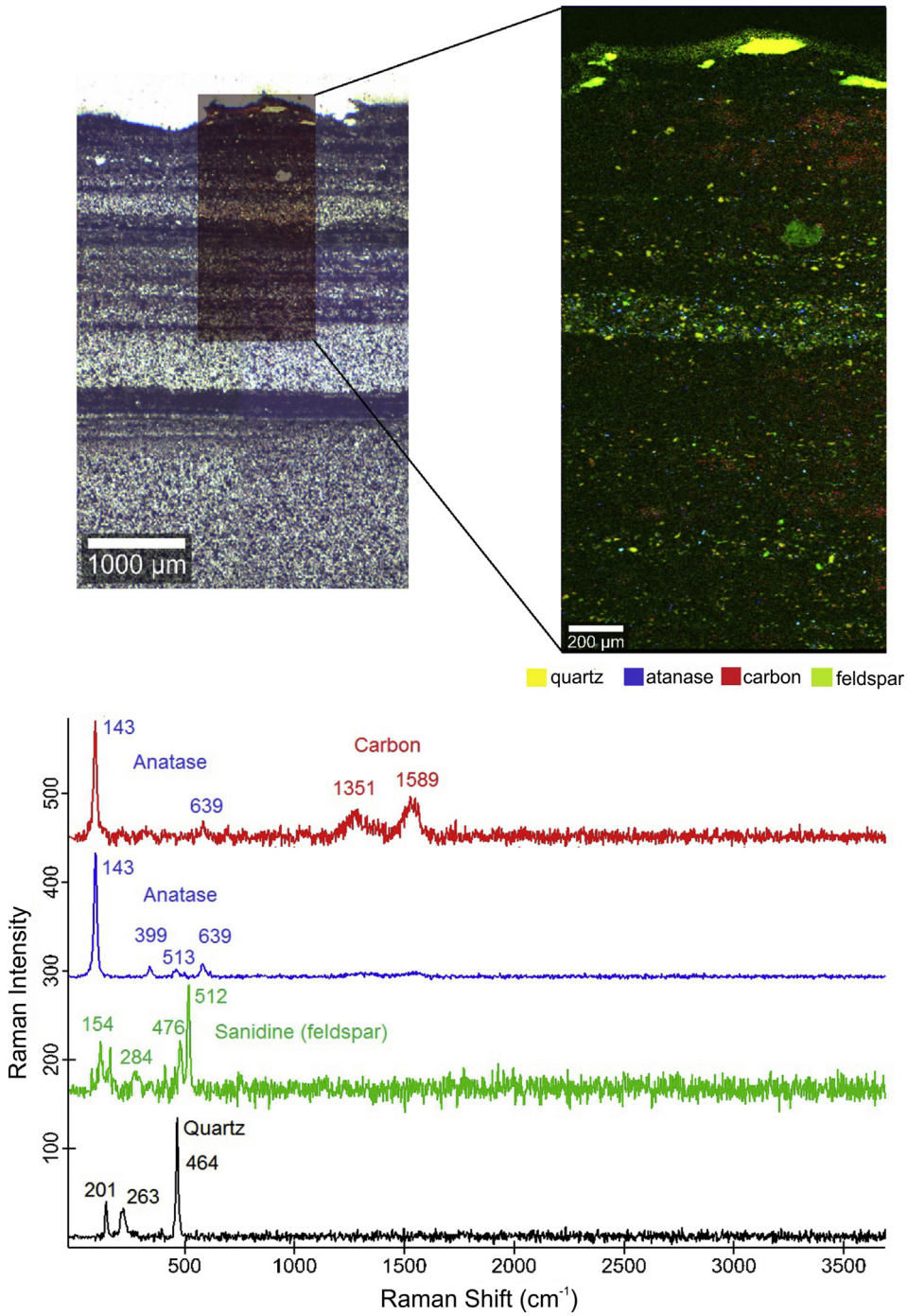

Fig. 5. Raman spectroscopy analysis in an area of 1 × 2.5 mm of the sample (LPP-0041). Elemental map shows the distribution of quartz (yellow), anatase (blue), carbon (red) and feldspar (green). In the light layers quartz grains predominate, while in the dark layers anatase and carbon predominate. Raman spectra with signature peak shifts for anatase at 143, 399, 513 and 639 cm^{-1}; for kerogen at 1351 and 1589 cm^{-1}; for feldspar (sanidine) at 154, 284, 476 and 512 cm^{-1} and for quartz at 201, 263 and 464 cm^{-1}. (For interpretation of the references to colour in this figure legend, the reader is referred to the web version of this article.)

4.7. Rock magnetic analysis

Rock magnetic analysis of the samples were performed mainly in the dark laminae (see Fig. 7). The isothermal remanent magnetization curves - IRM (Fig. 7A) and hysteresis loop of bulk samples (Fig. 7B) show two different magnetic phases, one with a low coercivity phase and the other with a high coercivity phase, which are probably magnetite and hematite respectively. In this case, the low coercivity phase presents the major contribution for the magnetization. The first order reversal curves - FORC diagram for the bulk sample (Fig. 7C) shows a slight central distribution. Low temperature data (FC/ZFC curves) show that the Verwey transition (Tv) has two distinct peaks at 100 and 120 K (Fig. 7D).

The IRM acquisition curve (Fig. 7E) and hysteresis loop (Fig. 7F) for extracted magnetic materials show higher values in comparison with the bulk sample. It suggests that the extracted material is dominated by low coercivity minerals. The FORC diagrams (Fig. 7G) show a distribution that is coherent with small magnetite crystals, but we cannot identify the central ridge distribution typically observed for biogenically-produced magnetite.

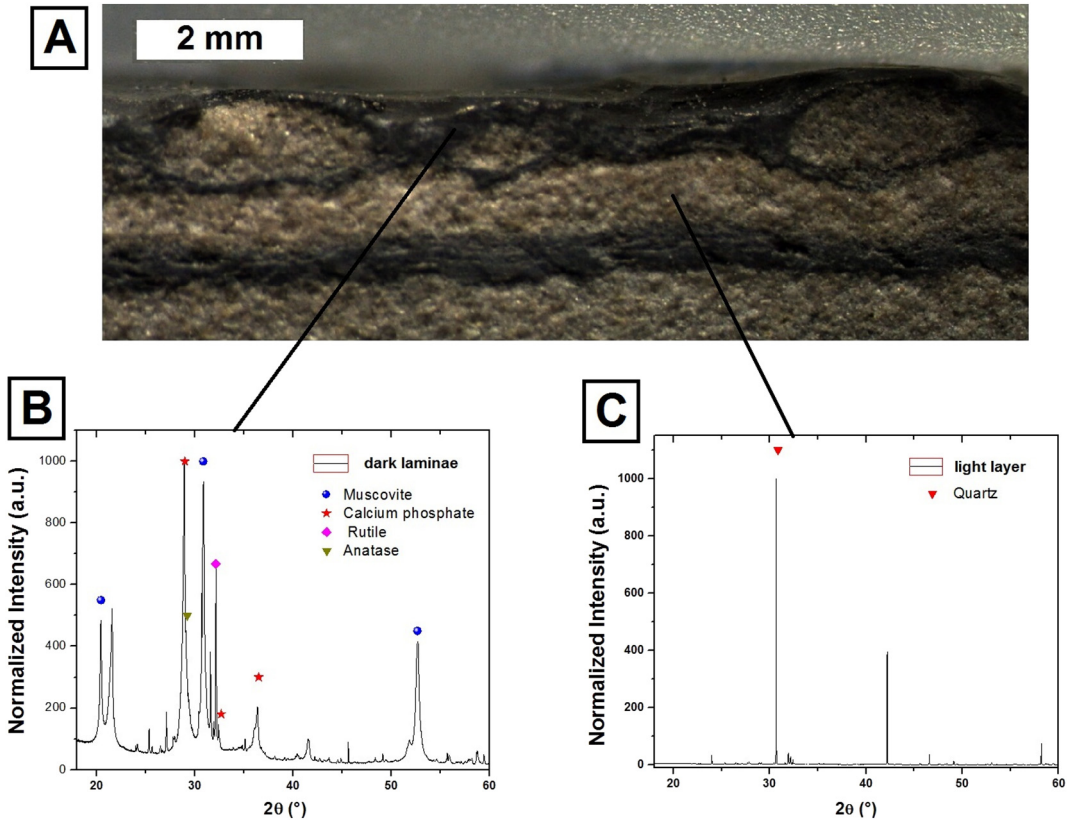

Fig. 6. (A) Analyzed sample (LPP-0040) showing the dark laminae and light layer; (B) diffractogram from the dark laminae, showing the mineral phases muscovite, calcium phosphate, rutile and anatase; (C) diffractogram from the light layer, showing the alpha-quartz mineral phase.

The low temperature magnetic results suggest that part of the magnetic mineralogy is composed of abiogenic magnetite (peak at 120 K) that can be interpreted as having a detrital origin. Nevertheless, the 100 K peak of Verwey transition indicates that some fraction of the abiogenic iron oxides was transformed into biogenic magnetite (Chang et al., 2016). Although there were episodes of anoxic conditions for the microorganisms after burial by sediments, there is no magnetic signal of sulfide minerals such as pyrite or greigite. The absence of these minerals may exclude the possibility of sulfate reduction activity (in the formation of magnetite), corroborating the magnetic analysis that also did not show any magnetic signature of iron sulfide.

5. Discussion

5.1. Microbially-induced sedimentary structures in the Itu Rhythmite

The dark laminae have been interpreted as mudstones (Rocha-Campos, 2002) or shale (Caetano-Chang and Ferreira, 2006). However, the analyses presented here show a significant presence of organic matter in the dark laminae. Iron minerals and anatase in combination with fossil bacterial extracellular polymeric substance (EPS) are preserved. Different macroscale MISS including wrinkle structures, levelled ripple marks, sinoidal structures, and gas domes point towards a dense colonization of the bottom of the water body by benthic microbiota. In analogous glacial deposits at the Mafra Formation (southern Brazil), Netto et al. (2008) observed microbially-induced wrinkle structures that strongly resemble those presented here from the Itu rhythmites. Also observed was the common occurrence of these structures with ichnofossil trace makers (*Diplichnites gouldi*), suggesting a close link between them. Netto et al. (2008) associated the sediment deposition over the microbially-induced wrinkle structures with periodic drainage of some shallow lakes, which can create freshwater marshes that may have partially dried up in some periods. Recently, Noll and Netto (2018) observed MISS related to epibenthic microbial mats in the rhythmites of the Rio do Sul Formation (Itararé Group), indicating low hydrodynamic and quiescent periods between the depositional events. Freshwater-terrestrial trace fossils were found in association with MISS in the Rio do Sul Formation.

As shown in the SEM/EDS analysis, the smooth biofilm surface that enveloped feldspar and quartz grains, plus the carbon detected in these envelopes, point to EPS fossilized in the dark layers. The EPS may be the major contributor to organic carbon in sediments (Decho, 2000).

In addition, the presence of iron primarily in the dark MISS laminae is remarkable. This iron presented a magnetic behavior compatible to biogenic magnetite, although there are two different magnetic phases in the dark layers (hematite and magnetite). Results of low temperature

Table 3
Reference diffraction pattern of crystalline inorganic phases identified in the dark and light layers, through the application of X-ray diffraction, excited with 7 keV.

Mineral	Reference code (ICDD[a])	Mineral name	PDF index name/ICDS name	Empirical formula	Chemical formula
Muscuvite	00–007-0042	Muscovite-3 *T*	Potassium Aluminum Silicate Hydroxide	$A_{l2\cdot9}0H_2KO_{12}Si_{3.10}$	$(K, Na)\ (Al, Mg, Fe)_2\ (Si_{3.1}A_{l0.9})\ O_{10}\ (OH)_2$
Calcium phosphate	00–009-0363	Calcium Phosphate	Calcium Phosphate	CaO_6P_2	$Ca(PO_3)_2$
Rutile	01–088-1174	Rutile - synthetic	Titanium Oxide	O_2Ti	TiO_2
Anatase	01–083-2243	Anatase - synthetic	Titanium Oxide	O_2Ti	TiO_2

[a] ICDD — International Centre for Diffraction Data.

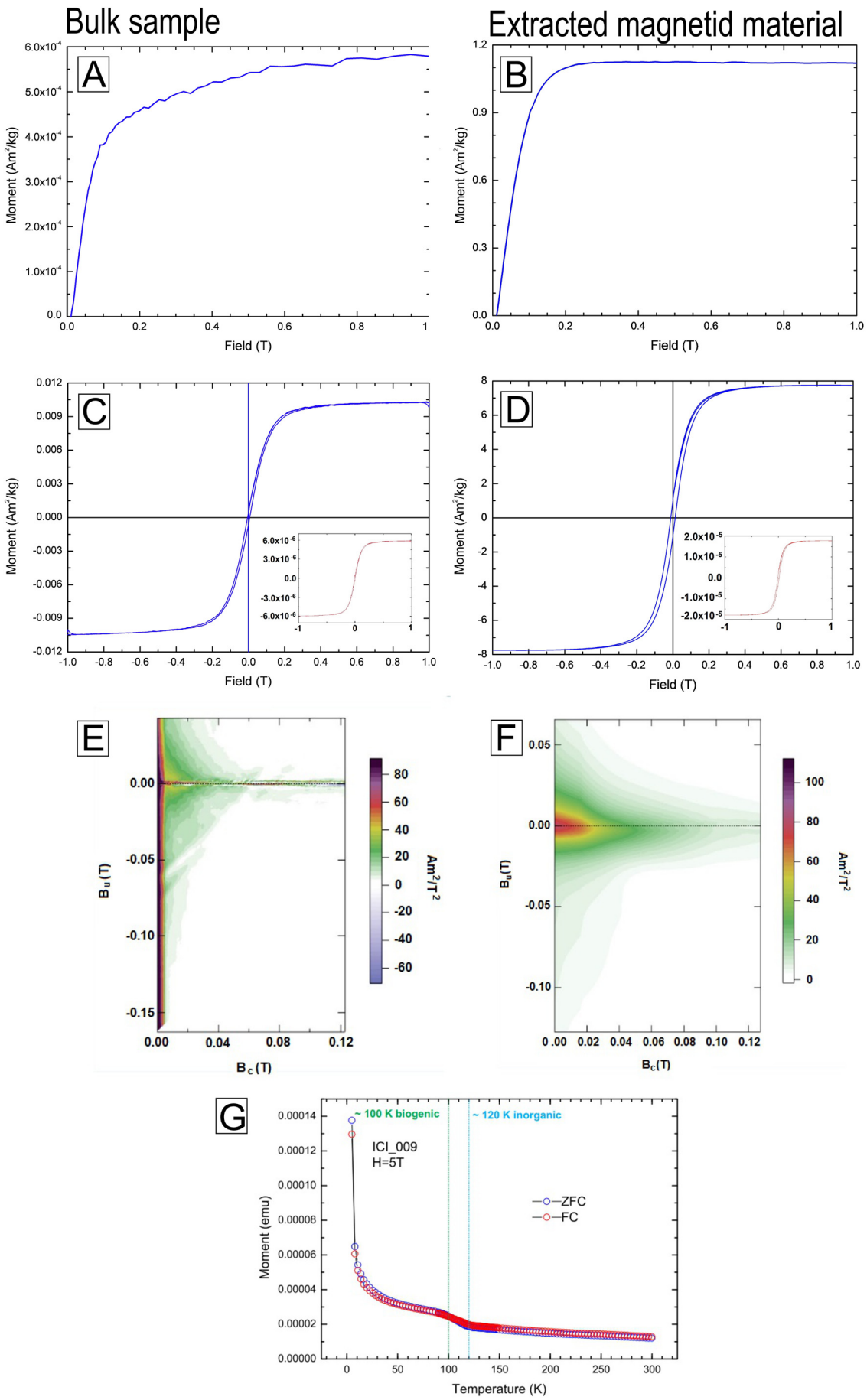
Bulk sample
Extracted magnetid material
A
B
C
D
E
F
G
Moment (Am²/kg)
Field (T)
Moment (emu)
Temperature (K)
~ 100 K biogenic
~ 120 K inorganic
ICI_009
H=5T
ZFC
FC
Bu (T)
Bc (T)
Am²/T²

measurements suggest that part of low coercivity phase (i.e., magnetite) is actually biogenic magnetite.

5.2. Hypotheses for a microbially-induced Fe mineral precipitation

In μ-XRF maps, the iron is distributed plane-parallel in the dark laminae. Microscopically, the iron is generally found in the biofilm in the samples, in areas of high organic matter concentration. In other areas outside the dark laminae, as in the light layers, there is little or no iron. This suggests a relation between the biofilms and iron precipitation. Many microorganisms reduce or oxidize iron in their metabolism (Konhauser and Riding, 2012), or produce magnetite by intracellular or extracellular mechanisms. Magnetotactic bacteria (MTB) can precipitate iron in a biologically-controlled way, forming intracellular magnetite, the magnetosomes, which allow the bacterial cells to align themselves along the magnetic field and to reach the optimal position in the water column with respect to chemical gradients (Blakemore, 1975). Another kind of bacteria, such as Fe(III)-reducing bacteria, can produce extracellular crystals of magnetite, in a biologically-induced way (Roh et al., 2006; Moon et al., 2007; Konhauser and Riding, 2012). The processes of iron biomineralization can influence the crystallographic and magnetic properties of these minerals (e.g., Vali and Kirschvink, 1991; Thomas-Keprta et al., 2000; Abrajevitch et al., 2016), allowing us to differentiate between these minerals according to their origin (biogenic or inorganic precipitation), using techniques such as X-Ray diffraction (Thomas-Keprta et al., 2000) or rock magnetic techniques (Egli, 2004). Here, we applied the magnetic techniques in combination with morphological biosignatures, such as EPS textures in SEM images, to detect the biogenicity of iron minerals in the dark laminae.

Glacial inputs can carry iron particles, which can be stabilized by inorganic or organic processes (von der Heyden et al., 2012). In the modern glacial lakes of Clearwater, Silver and others in the Canadian province of Ontario, microbial mats are produced by iron bacteria (Fortin et al., 1993). Ferrous ions in the surrounding water may foster the development of iron-metabolizing microbes (Fortin et al., 1993; Schieber and Glamoclija, 2007). Iron-oxidizing bacteria, such as *Gallionella* and *Leptothrix*, can oxidize Fe(II) according the reaction $Fe^{2+} + 0.25O_{2(aq)} + 2.5H_2O \rightarrow Fe(OH)_{3(s)} + 2H^+$ (Schieber and Glamoclija, 2007). Iron-reducing bacteria can use the Fe ions from ferrihydrite ($Fe_2O_3.0, 5H_2O$), the most common bio-available form of Fe(III) oxide in nature. The magnetite particles may be a result of the reaction during the dissimilatory iron reduction through a coupled biotic-abiotic process (Hansel et al., 2003). One of these reactions is the reduction of iron oxide to nanocrystals of ferromagnetic magnetite by the action of hyperthermophilic iron-reducing bacteria (Lovley et al., 1987).

Another hypothesis for the origin of magnetite in the dark layers is related to MTB. These microorganisms preferentially live under specific redox conditions in the oxic-anoxic transition zone (Bazylinski and Moskowitz, 1997) and present octahedral crystals of magnetite arranged in chains inside their cells, the magnetosomes. These crystals range from 19 to 136 nm in length and 14 to 112 nm in width (Lins and Farina, 1998). When the bacteria were buried, their magnetosomes can be preserved in the rock record, but diagenetic alteration and degradation of organic matter can rearrange the chain of the magnetosomes (Kopp and Kirschvink, 2008; Amor et al., 2015). In our study, TEM analyses showed isolated octahedral crystals. They are not arranged in chains. However this disarray may be an artefact of the destructive ferromagnetic mineral extraction process which includes mechanical crushing and extraction with acid. Elongated magnetite crystals may be related to specific magnetofossils, such as those originated from MTB found in a borehole in Quaternary sediments from the Atlantic Coastal Plain of New Jersey (Schumann et al., 2008). The crystals found in dark layers are approximately 200 to 250 nm in length. Schumann et al. (2008) describe their longest magnetofossil as 580 nm. Other modern examples from the Bahamas are up to 170 nm in length. According to Schumann et al. (2008), such magnetosomes occur as isolated features or as aggregates of originally isolated crystals; this is in contrast with most magnetosomes of MTB, which are arranged in chains. Although the possible existence of magnetofossils should not be excluded, the evidence for this occurrence in TEM images is not sufficient to show that there was an expressive participation of MTB in the iron deposits of the dark laminae. Therefore, the hypothesis of extracellularly-precipitated magnetite by iron reducing bacteria is more suitable, since the iron is distributed throughout the length of the microbial mat in the dark laminae, not locally distributed. This may denote high rates of mineral production consistent with a well-developed microbial mat. The lack of evidence of magnetite in chains in the bulk samples analyzed by TEM make the hypothesis of mineral precipitation by a biologically-induced way in extracellular mechanisms more suitable. In addition, the presence of myriapod trace-fossils (invertebrates which need oxygen to breathe) in the dark laminae corroborates with the shallow depth of the water body, which represents an environment more likely for the proliferation of iron reducing-bacteria.

The anatase (TiO_2) distribution concurs with the biofilm texture, suggesting the possibility of this mineral resulting from bio-precipitation. Bower et al. (2015) obtained anatase bioprecipitation under simulated conditions similar to early diagenesis, in incubation experiments of cyanobacteria in sandy environments.

5.3. Ichnofossils

The invertebrate ichnofossils such as *Diplichnites gouldi* found in the surface of the dark laminae are very well preserved, which allows us to observe important details for its identification. The good preservation of the ichnofossils is in part due to the fine-grained nature of the dark sediment, but also because of the EPS of the biofilms, whose role in the trapping and binding of fine sediments biostabilizes the system and attenuates the effects of erosion. According to Fernandes and Carvalho (2005), two ichnogenus are abundant in the rocks of the Itararé Group: *Isopodichnus* Bornemann (1889) and *Diplichnites* Dawson (1873), possibly attributed to arthropods myriapods (Draganits et al., 2001; Netto et al., 2008).

The wrinkle structures occur where apparently some arthropod has moved over the microbial mat, causing dragging and distortion of the mat without breaking. This leads to the preservation of trace fossils in high relief forms.

The depth of the water body was variable during the final time of deposition. Cracks in the dark laminae are evidence of subaerial exposure of the water body bottom and indicate that there may have been periods of water shortage in the system. The shallow water shortly before and after an exposure event would be opportune for intense foraging by invertebrates. Lima et al. (2015), in analyses of similar ichnofossils from the Itararé Group in Santa Catarina State (southern Brazil), concluded that the tracks were produced by arthropods during colonization of ephemeral, shallow water bodies filled by fresh water from glacier melt. Gandini et al. (2006) and Netto et al. (2008) identified an ichnofossiliferous assemblage in the glacial deposits of the Itararé

Fig. 7. Magnetic analysis in the bulk sample and in the extracted magnetic material. (A) isothermal remnant magnetization curves (IRM) of the bulk sample; (B) isothermal remnant magnetization curves (IRM) of the extracted magnetic material; (C) hysteresis loop of the bulk sample; (D) hysteresis loop of the extracted magnetic material; (E) first order reversal curves (FORC) diagram of the bulk sample, showing a slight central ridge distribution typical of biogenic magnetite; (F) first order reversal curves (FORC) diagram of the extracted magnetic material without the central ridge distribution related to the biogenic magnetite, although it indicates a very small crystal size; (G) low-temperature magnetization measurements after zero-field cooled (ZFC) and field-cooled (FC) conditions (FC/ZFC curves), showing the Verwey transition in peaks at 100 and 120 K.

Group, which contains mollusk tracks and trails attributed to crustaceans such as *Protovirgularia* isp., *Diplichnites gouldi*, *Diplopodichnus biformis*, *Maculichna varia* and *Umfolozia sinuosa*. Shallow excavations of vermiform organisms, generated on substrates with wrinkle marks associated with microbial mats, are attributed to the ichnospecies *Cochlichnus anguineus*, *Hormosiroidea meandrica* and *Treptichnus* isp. Resting impressions of arthropods such as *Gluckstadella cooperi*, are also present in fine and dark laminae of the glacial rhythmic deposits of the south and southeast regions of Brazil, such as the Itu rhythmites.

Gandini et al. (2006) and Netto et al. (2008) also established the characteristics of life habits in relation to the organisms which produce the different tracks and trails in the Itararé Group. According to these authors, the dominance of trails of terrestrial and aquatic arthropods preserved on the wrinkles and shallow excavations, suggests a life habit of foraging in the microbial mats. The presence of myriapod trails in the rhythmites suggests that the water bodies formed during warmer periods were shallow.

Netto et al. (2008) suggested two ichnofacies for the southern region of Brazil to explain the occurrences of the ichnofauna present in the Itararé Group. A Mermia ichnofacies, comprised of a sequence of shallow freshwater with the dominance of *Cochlichnus anguineus* trails, *Cruziana* cf. *problematica*, *Gordia arcuata*, *Gordia marina*, *Hormiroidea meandrica*, *Rusophycus* cf. *carbonarius* and *Treptichnus pollardi*, as well as *Undichnia consulca*, an intermittent rusophyciform traces; and an atypical *Scoyenia* ichnofacies composed of the ichnospecies *Diplichnites gouldi* and *Diplichnites biformis*, whose tracks were preserved together with the wrinkles structures induced by microorganisms, suggesting a coastal environment of brackish water.

5.4. Modern analogues

Microbial mats can develop in a wide range of settings under favorable conditions, including those covered by ice (Simmons et al., 1993; Noffke, 2010). The biological mechanisms of iron cycling and the role of iron-oxidizing and the iron-reducing bacteria in glacial environments are still poorly understood (Emerson et al., 2015; Nixon et al., 2017). Nixon et al. (2017) evaluated the prevalence of iron-reducing bacteria in several glacial settings, such as Russell Glacier (Greenland) and Lower Wright Glacier (Antarctica), observing an increase in the rate of iron reduction at low temperatures.

Seasonal deposits (varvites) with biological participation are not uncommon. Chutko and Lamoureux (2009) evaluated a biolaminated sedimentary sequence from a high Arctic coastal freshwater lake, which consists of alternating clastic and organic layers caused by climate seasonality. Chutko and Lamoureux (2009) proposed that during the winter, ice would cover the lake's surface and inhibit the proliferation of microbial mats. In the months of warmer springs, cyanobacteria are favored and can proliferate. During the summer, when the ice melts, the sediments are deposited, covering the mats and inhibiting their activity again, giving rise to the clastic deposits.

A similar model can be constructed for the Itu rhythmite. The couplets in Itu may reflect seasonality similar to that described by Chutko and Lamoureux (2009) from their high Arctic lake. The layers towards the top of the rock succession include more kerogen than the layers towards the base, showing that at this stage, biological processes were prominent in relation to physical sedimentary processes. Overall, the thinner top layers compared to that of the near-base layers points towards a shallow depth of the lake and a lower input rate of sediments. The dark-light couplets may record different depositional processes for different seasons (winter, summer, spring and autumn):

(A) During the cold periods (winter) when the ice covered the surface of the water body, the low temperature reduced bacterial productivity rate. In this season, dark laminae deposition occurred only by fallout of fine sediments (clay/silt) when turbidity in the water body was low, with low participation of microorganisms (Fig. 8A).
(B) Towards the periods of mild temperatures (autumn and spring), the increasing temperature melts the ice on the surface, and microorganisms increase their productivity. Because the lake water was still clear, productivity was at its maximum during that time. The microbial mats accumulate biomass, which later contributed to the formation of the dark laminae (Fig. 8B).
(C) In the mild weather periods (summer), the lack of an ice cover allows the increase of sediment influx from the surroundings. The level of the water body may have risen due to the melting of the glacier. The sediments derived from the surroundings by wind and water transport constitute the light layers (Fig. 8C).

5.5. Implications for a depositional model

The Itu deposits are classified as varve-type, and formed as a result of annual depositions of couplets in a proglacial environment with increasing marine influence (Caetano-Chang and Ferreira, 2006). According to paleomagnetic studies by Franco et al. (2012), the average rate of sedimentation was 41.4 m/My. Through detailed petrographic studies in the Itu rhythmites, Caetano-Chang and Ferreira (2006) proposed that the "varvite" denomination for a large part of these deposits may be inadequate; only the top of the Itu rhythmites has a periodicity consistent with one year deposition for one lithological couplet. The authors argue that for most of the Itu rhythmites the deposition of the light layers depends on several factors, such as sediment supply in warmer seasons and lake hydrodynamic conditions, and may result from deposition of low density flux (underflow). The authors also argue that the dark laminae were deposited sporadically in rigorous winters at irregular intervals, when the lake surface was frozen. Considering that biological activity influenced mineral precipitation during the deposition of the dark laminae, our study corroborates the non-periodicity of one year per lithological couplet.

Anderson and Dean (1988) showed that, if there is high iron content, the oxidation and flocculation may form laminae in addition to the seasonal stratification processes. Although it is a rare event, higher organic productivity in longer periods of good conditions for microbial development, such as the proliferation of microorganisms capable to reduce or oxide iron, can originate laminae in a rhythmic deposit (O'Sullivan, 1983; Anderson and Dean, 1988). According O'Sullivan (1983), there are several occurrences of ferrogenic varves: Greenleaf Lake, Canada (Cwynar, 1978), Hell's Kitchen Lake, U.S.A. (Swain, 1978), Pyhäjärvi, Finland (Kukkonen and Tynni, 1970), and Rudetjärn, Sweden (Renberg, 1978), among others.

For the model presented here, we caution against defining an annual deposition of the couplets, at least for the layers where the microorganisms contributed to mineral precipitation. This is because, in high temperatures, iron bacteria productivity is favored, while at low temperatures this rate decreases (Koehler et al., 2010), but does not cease to exist. Therefore, the deposition of iron would be more intense during warmer periods and less intense during colder periods. According to dos Santos et al. (1996), the glaciation had its maximum during the interval between the Pennsylvanian and Lower Permian, decreasing in the Asselian, but Cagliari et al. (2016) showed that the end of glaciation occurred at the top of late Pennsylvanian (Ghzelian), at least in the southern portion of the Paraná Basin. The time of melting of the ice masses was irregular along the eastern margin of the Paraná Basin, which includes the Itu rhythmite (dos Santos et al., 1996). We suggest that the alternating bedding of light and dark layers may not be related directly to a seasonal pattern, but controlled by the microbial mat development and the environmental conditions that control its growth, since the mat development is dependent on several factors, such as solar

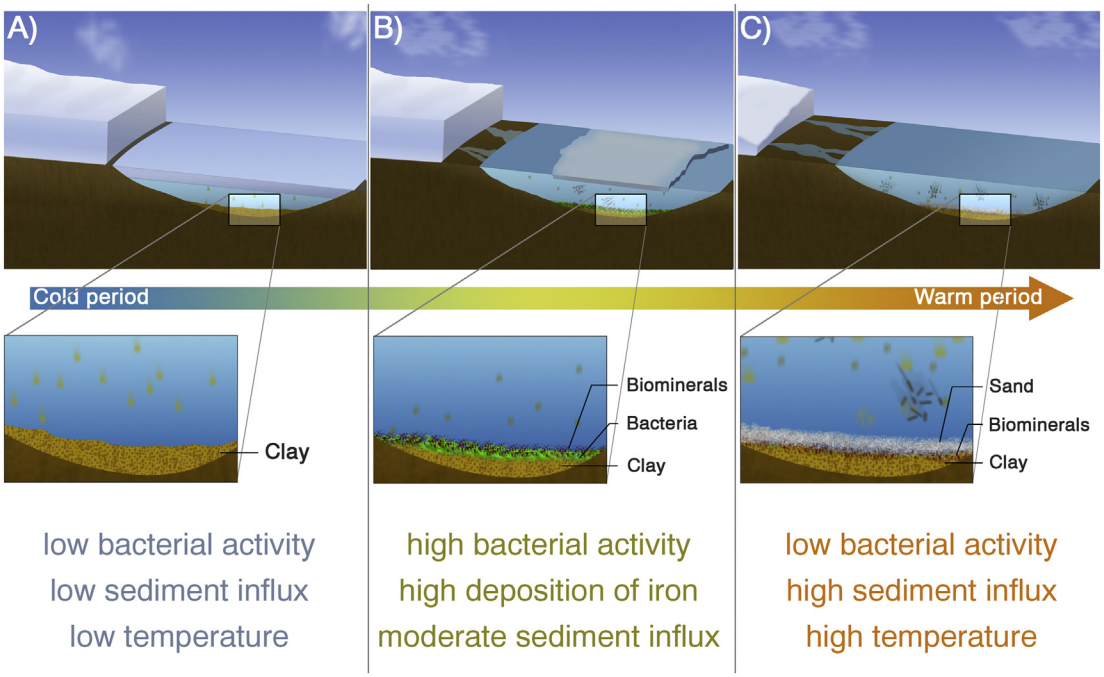

Fig. 8. Depositional model for the last deposition of Itu rhythmites, considering the presence of microorganisms and the deposition of biologically induced minerals to the composition of the dark laminae. (A) cold periods, with ice covering the lake's surface, preventing sediments from being transported into the lake. The cold temperatures decrease the bacterial activity; therefore, the deposition of the dark laminae occurs only by fallout of fine sediment that was in suspension in the water; (B) mild temperatures, with the lake partly covered by ice (melting glaciers). The influx of sediment increases in comparison to the cold periods, but does not yet prevent the growth of microbial mats on the bottom of the lake. In these periods, the bacterial productivity reaches its maximum and the dark laminae are formed by the combination of mineral bio-precipitation, organic matter production and fine sediment deposition by decantation. This process continues until it is terminated by the increase of the sediment influx to the bottom of the lake; (C) relatively warmer periods during which the lake is not covered by ice; the maximum sediment influx buried the microbial mats, and constitutes the light layers.

intensity, temperature and sediment influx. Noll and Netto (2018) argue that the main control of the depositional system in glacigenic rhythmites in the Trombudo Central region of the Rio do Sul Formation (Itararé Group) was given by cycles of advance and retreat of glaciers during interglacial cycles. In this case, the deposits that represent the light layers were formed during seasonal deglaciation periods, while the dark layers should represent the quiescent periods during climatic amelioration, when the glacier input was minimal and the sediment influx decreased.

Considering the biological activity in the deposition of the dark laminae in Itu rhythmites, the periodicity of each layer could be also controlled by bacterial productivity in periods of quiescence, in a similar context to that presented by Noll and Netto (2018) for Rio do Sul Formation rhythmites. A certain period with ideal conditions is necessary for the microorganisms to proliferate and to create a biofilm of recognizable thickness. These ideal conditions can vary according to the sediment influx, which is dependent on the retention of sediments by glaciers. The necessary period of time for this to occur may be greater or smaller than required for mechanical deposition (only by gravity), such as the classical depositional model of the Itu rhythmites (one year per lithological couplet).

6. Conclusions

The use of the multi-method approach (petrology, EPMA, SEM/EDS, XRF, XRD, TEM, Raman spectroscopy and rock magnetism analysis) was applied to test the biogenicity of the iron minerals in the dark of the Itu rhythmites. Results indicate the co-occurrence of microbial mats and invertebrates of possibly mat-grazing benthos in the top of the Itu rhythmite succession. In microscopic section, the MISS includes dark laminae that comprise organic matter and bio-precipitated minerals. Taking this evidence together, we suggest that the dark laminae are of microbial origin. Considering that bacteria in low temperatures need quiescence in order to grow and form microbial mats, in addition to the fact that the microbial mat development may have masked any seasonal fluctuations in the depositional pattern, the periodicity of one year per couplet may not be a sufficient suitable explanation for the upper portion of this rock succession. Because of this, the classical model for deposition of varve-type deposits for the Itu rhythmites needs to be reconsidered. In addition, this study suggests the need to investigate the presence of biominerals in similar depositional systems elsewhere, since its detection can mean significant changes in their paleoenvironmental interpretations and their depositional systems.

Acknowledgments

We acknowledge the comments and suggestions of Kenneth Kodama and Renata Guimarães Netto and, the editorial work of Sunoj Sankaran and Jasper Knight for the valuable criticisms and efforts for the improvement of this manuscript. The authors would like to thank the Brazilian Synchrotron Light Laboratory (LNLS/CNPEM) and the Brazilian Nanotechnology Laboratory (LNNano/CNPEM) for the availability of the facilities (μ-XRF, XRD2, SEM/EDS and TEM) through the approval of the proposals no 20150076, no 20160071, SEM 23265 and ME 22557, respectively; the Geophysical Laboratory from Carnegie Institution of Science (Washington, DC) for the availability of microprobe and Raman spectrometer; the Paleomagnetism Laboratory of University of São Paulo (USPMag), Brazil; the Brazilian Federal Agency for Support and Evaluation of Graduate Education - CAPES Foundation and the PDSE Program for the financial support and scholarship; and the São Paulo Research Foundation – FAPESP (grant no 2016/20927-0 and no 2016/06114-6) for funding this project. The authors also thank CAPES (grant AUXPE 2043/2014) and CNPq (National Council for Scientific and Technological Development, grant no 454609/2014-0 and no 424367/2016-5) and Serrapilheira Institute (project number G-1709-20205).

References

Abrajevitch, A., Kondratyeva, L.M., Golubeva, E.M., Kodama, K., Hori, R.S., 2016. Magnetic properties of iron minerals produced by natural iron- and manganese-reducing groundwater bacteria. Geophysical Journal International 206, 1340–1351.

Amor, M., Busigny, V., Durand-Dubief, M., Tharaud, M., Ona-Nguema, G., Gélabert, A., Alphandéry, E., Menguy, N., Benedetti, M.F., Chebbi, I., Guyot, F., 2015. Chemical signature of magnetotatic bacteria. Proceedings of the National Academy of Sciences 112, 1699–1703.

Anderson, R.Y., Dean, W.E., 1988. Lacustrine varve formation through time. Palaeogeography, Palaeoclimatology, Palaeoecology 62, 215–235.

Bazylinski, D.A., Moskowitz, B.M., 1997. Microbial biomineralization of magnetic iron minerals: microbiology, magnetism and environmental significance. Reviews in Mineralogy and Geochemistry 35, 181–223.

Blakemore, R., 1975. Magnetotactic bacteria. Science 190, 377–379.

Bornemann, J.G., 1889. Über den Bintsandstein in Deutschland und seine Bedeutungfürdie Trias. Beiträge zur Geologie und Paläontologie 1, 1–61.

Bower, D.M., Hummer, D.R., Steele, A., Kyono, A., 2015. The co-evolution of Fe-oxides, Ti-oxides, and other microbially induced mineral precipitates in sandy sediments: understanding the role of cyanobacteria in weathering early diagenesis. Journal of Sedimentary Research 85, 1213–1227.

Caetano-Chang, M.R., Ferreira, S.M., 2006. Ritimitos de Itu: petrografia e considerações paleodeposicionais. Universidade Estadual Paulista Júlio de Mesquita Filho, UNESP, Revista Geociências 25, 345–358.

Cagliari, J., Philipp, R.P., Buso, V.V., Netto, R.G., Hillebrand, P.K., Lopes, R.C., Basei, M.A.S., Faccini, U.F., 2016. Age constraints of the glaciation in the Paraná Basin: evidence from new U–Pb dates. Journal of the Geological Society 173, 871–874.

Caputo, M.V., Melo, J.H.G., Streel, M., Isbell, J.L., 2008. Late Devonian and Early Carboniferous glacial records of South America. In: Fielding, C.R., Frank, T.D., Isbell, J.L. (Eds.), Resolving the Late Paleozoic Ice Age in Time and Space. Geological Society of America Special Paper 441, p. 13.

Chang, L., Heslop, D., Roberts, A.P., Rey, D., Mohamed, K.J., 2016. Discrimination of biogenic and detritical magnetite through a double Verwey transition temperature. Journal of Geophysical Research - Solid Earth 121, 3–14.

Chutko, K.J., Lamoureux, S.F., 2009. Biolaminated sedimentation in a High Arctic freshwater lake. Sedimentology 56, 1642–1654.

Cwynar, L.C., 1978. Recent History of Fire and Vegetation from Laminated Sediment of Greenleaf Lake, Algonquin Park, Ontario. Canadian Journal of Botany 56, 10–21.

Dawson, J.W., 1873. Impressions of footprints of aquatic animals and imitative markings, on Carboniferous rocks. American Journal of Science 51, 6–24.

Decho, A.W., 2000. Microbial biofilms in intertidal systems: an overview. Continental Shelf Research 20, 1257–1273.

Dickinson, W.R., 1970. Interpreting detrital modes of graywacke and arkose. Journal of Sedimentary Petrology 40, 695–707.

d'Orbigny, A., 1842. Voyage dans l'Amérique méridionale (le Brésil, la République oriental de l'Uruguay, la République Argentine, la Patagonie, la République du Chili, la République de Bolivia, la République du Péron) exécuté pendant les annees 1826, 1827, 1829, 1830, 1831, 1832, et 1833. 3. Pitois-Levrault (Paris), Levrault Strasbourg, p. 188.

dos Santos, P.R., Rocha-Campos, A.C., Canuto, J.R., 1996. Patterns of late Paleozoic deglaciation in the Paraná Basin, Brazil. Palaeogeography, Palaeoclimatology, Palaeoecology 125, 165–184.

Draganits, E., Braddy, S.J., Briggs, D.E.G., 2001. A Gondwanan coastal arthropod ichnofauna from the Muth Formation (Lower Devonian, Northern India): paleoenvironment and tracemaker behaviour. Palaios 16, 126–147.

Egli, R., 2004. Characterization of individual rock magnetic components by analysis of remanence curves, 1. Unmixing natural sediments. Studia Geophysica et Geodaetica 48, 391–446.

Emerson, D., Scott, J.J., Bernes, J., Bowden, W.B., 2015. Microbial iron oxidation in the arctic tundra and its implications for biogeochemical cycling. Applied and Environmental Microbiology 81, 8066–8075.

Fernandes, A.A.S., Carvalho, I.S., 2005. The ichnofossils from the Brazilian Permian Varvites. Abstract, Abstracts of Gondwana 12. Academia Nacional de Ciências, Mendoza, p. 150.

Fortin, D., Tessier, A., Leppard, G.G., 1993. Characteristics of lacustrine iron oxyhydroxides. Geochimica et Cosmochimica Acta 57, 4391–4404.

Franco, D.R., Hinnov, L.A., Ernesto, M., 2012. Millennial-scale climate cycles in Permian–Carboniferous rhythmites: Permanent feature throughout geologic time? Geology 40, 19–22.

Gandini, R., Netto, R.G., Souza, P.A., 2006. Paleoicnologia e a palinologia dos ritmitos do Grupo Itararé na pedreira de Águas Claras (Santa Catarina, Brasil). Gaea - Journal of Geoscience 3, 47–59.

Gerdes, G., Klenke, T., Noffke, N., 2000. Microbial signatures in peritidal siliciclastic sediments: a catalogue. Sedimentology 47, 279–308.

Giles, C., Yokaichiya, F., Kycia, S.W., Sampaio, L.C., Ardiles-Saravia, D.C., Franco, M.K.K., Neuenschwander, R.T., 2003. High-resolution X-ray diffraction beamline at the LNLS for the study of charge, orbital and magnetic structures. Journal of Synchrotron Radiation 10, 430–434.

Hansel, C.M., Benner, S.G., Neiss, J., Donalkova, A., Kukkadapu, R.K., Fendorf, S., 2003. Secondary mineralization pathways induced by dissimilatory iron reduction of ferrihydrite under advective flow. Geochimica et Cosmochimica Acta 67, 2977–2992.

Harrison, R.J., Feinberg, J.M., 2008. FORCinel: an improved algorithm for calculating first-order reversal curve (FORC) distributions using locally-weighted regression smoothing. Geochemistry, Geophysics, Geosystems 9, Q05016. https://doi.org/10.1029/2008GC001987.

Ianuzzi, R., 2010. The flora of Early Permian coal measures from the Paraná Basin in Brazil: a review. International Journal of Coal Geology 83, 229–247.

Koehler, I., Konhauser, K., Kappler, A., 2010. Role of microorganisms in banded iron formation. In: Loy, A., Mandl, M., Barton, L.L. (Eds.), Geomicrobiology: Molecular and Environmental Perspective. Springer Science+Business Media B.V., Netherlands, pp. 309–324.

Konhauser, K., Riding, R., 2012. Bacterial biomineralization. In: Knoll, A.H., Canfield, D.E., Konhauser, K.O. (Eds.), Fundamentals of Geobiology. Blackwell Publishing, England, pp. 105–130.

Kopp, R.E., Kirschvink, J.L., 2008. The identification and biogeochemical interpretation of fossil magnetotactic bacteria. Earth-Science Reviews 86, 42–61.

Kukkonen, E., Tynni, R., 1970. Die Entwicklung des sees Pyhäjärvi in Sudfinnland in lichte von Sediment-und Diatomeenuntersuchungen. Acta Botanica Fennica 90, 1–36.

Lima, J.H.D., Netto, R.G., Corrêa, C.G., Lavina, E.L.C., 2015. Ichnology of deglaciation deposits from the Upper Carboniferous Rio do Sul Formation (Itararé Group, Paraná Basin) at central-east Santa Catarina State (southern Brazil). Journal of South American Earth Sciences 63, 137–148.

Lins, U., Farina, M., 1998. Magnetosome size distribution in uncultured rod-shaped bacteria as determined by electron microscopy and electron spectroscopic imaging. Microscopy Research and Technique 42, 459–464.

Lovley, D.R., Stolz, J.F., Nord, G.L., Phillips, E.J.P., 1987. Anaerobic production of magnetite by a dissimilatory iron-reducing microorganism. Nature 330, 252–254.

Lowenstam, H.A., 1981. Minerals formed by organisms. Science 211, 1126–1131.

Milani, E.J., Faccini, U.F., Scherer, C.M., Araújo, L.M., Cupertino, J.A., 1998. Sequences and stratigraphic hierarchy of the Paraná Basin (Ordovician to Cretaceous), Southern Brazil. Boletim do Instituto de Geociências da Universidade de São Paulo, Série Científica 29, 125–173.

Milani, E.J., Melo, J.H.G., Souza, P.A., Fernandes, L.A., França, A.B., 2007. Bacia do Paraná. Cartas Estratigráficas. Boletim de Geociências da Petrobrás 15, 265–287.

Montañez, I.P., Poulsen, C.J., 2013. The Late Paleozoic Ice Age: an Evolving Paradigm. Annual Review of Earth and Planetary Sciences 41, 629–656.

Moon, J.W., Roh, Y., Lauf, R.J., Vali, H., Yeary, L.W., Phelps, T., 2007. Microbial preparation of metal-substituted magnetite nanoparticles. Journal of Microbiological Methods 70, 150–158.

Netto, R.G., Balistieri, P.R.N.M., Lavina, E.L.C., Silveira, D.M., 2008. Ichnological signatures of shallow freshwater lakes in the glacial Itararé Group (Mafra Formation, Upper Carboniferous-Lower Permian of Paraná Basin, S Brazil). Palaeogeography, Palaeoclimatology, Palaeoecology 272, 240–255.

Nixon, S.L., Telling, J.P., Wadham, J.L., Cockell, C.S., 2017. Viable cold-tolerant iron-reducing microorganisms in geographically diverse subglacial environments. Biogeosciences 14, 1445–1455.

Noffke, N., 2010. Microbial Mats in Sandy Deposits. Elsevier, Amsterdam (196 pp.).

Noffke, N., Gerdes, G., Klenke, T., Krumbein, W.E., 1996. Microbially induced sedimentary structures — examples from modern sediments of siliciclastic tidal flats. Zentralblatt für Geologie und Paläontologie 1, 307–316.

Noffke, N., Gerdes, G., Klenke, Th., Krumbein, W.E., 2001. Microbially induced sedimentary structures — a new category within the classification of primary sedimentary structures. Journal of Sedimentary Research 71, 649–656.

Noll, S.H., Netto, R.G., 2018. Microbially induced sedimentary structures in late Pennsylvanian glacial settings: a case study from the Gondwanan Paraná Basin. Journal of South American Earth Sciences 88, 385–398.

O'Sullivan, P.E., 1983. Annually-laminated lake sediments and the study of Quaternary environmental changes — a review. Quaternary Science Reviews 1, 245–313.

Renberg, I., 1978. Paleolimnology and varve counts of the annually laminated sediments of lake Rudetjärn, Northern Sweden. Early Norland 11, 63–92.

Roberts, A.P., Heslop, D., Zhao, X., Pike, C.R., 2014. Understanding fine magnetic particle systems through use of first-order reversal curve diagrams. Reviews of Geophysics 52, 557–602.

Rocha-Campos, A.C., 2002. Varvito de Itú, SP: registro clássico da glaciação neopaleozóica. Sitios Geológicos e Paleontológicos do Brasil (SIGEP) 62, 147–154.

Roh, Y., Vali, H., Phelps, T.J., Moon, J.W., 2006. Extracellular Synthesis of Magnetite and Metal-Substituted Magnetite Nanoparticles. Journal of Nanoscience and Nanotechnology 6, 3517–3520.

Ruppert, E.E., Barnes, R.D., 2004. Invertebrate Zoology: A Functional Evolutionary Approach. Thomson-Brooks/Cole (989 pp.).

Schieber, J., Glamoclija, M., 2007. Microbial mats built by iron bacteria: a modern example from southern Indiana. In: Schieber, J., Bose, P.K., Eriksson, P.G., Banerjee, S., Altermann, W., Catuneau, O. (Eds.), Atlas of Microbial Mat Features Preserved within the Clastic Rock Record. Elsevier, Amsterdam, pp. 233–244.

Schumann, D., Raub, T.D., Kopp, R.E., Guerquin-Kern, J.L., Wu, T.D., Rouiller, I., Smirnov, A.V., Sears, S.K., Lücken, U., Tikoo, S.M., Hesse, R., Kirschvink, J.L., Vali, H., 2008. Gigantism in unique biogenic magnetite at the Paleocene-Eocene Thermal Maximum. Proceedings of the National Academy of Sciences 105, 17648–17653.

Simmons Jr., G.M., Vestal, J.R., Wharton Jr., R.A., 1993. Environmental regulators of microbial activity in continental Antarctic lakes. In: Green, W.J., Friedmann, E.I. (Eds.), Physical and Biogeochemical Processes in Antarctic Lakes. American Geophysical Union, Washington, DC, pp. 165–195.

Skinner, H.C.W., 2005. Biominerals. Mineralogical Magazine 69, 621–641.

Solé, V.A., Papillon, E., Cotte, M., Walter, P., Susini, J., 2007. A multiplatform code for the analysis of energy-dispersive X-ray fluorescence spectra. Spectrochimica Acta Part B: Atomic Spectroscopy 62, 63–68.

Souza, P.A., Félix, C.M., Pérez-Aguilar, A., Petri, S., 2010. Pennsylvanian palynofloras from the Itu rhythmites (Itararé Subgroup, Paraná Basin) in São Paulo State, Brazil. Revue de Micropaleontologie 53, 69–83.

Strehlau, J.H., Hegner, L.A., Strauss, B.E., Feinberg, J.M., Penn, R.L., 2014. Simple and efficient separation of magnetic minerals from speleothems and other carbonates. Journal of Sedimentary Research 84, 1096–1106.

Swain, A., 1978. Environmental changes during the past 2000 years in N-Central Wisconsin: analysis of pollen, charcoal and seeds from varved lake sediments. Quaternary Research 10, 55–68.

Thomas-Keprta, K.L., Bazylinski, D.A., Kirschvink, J.L., Clemett, S.J., Mckay, D.S., Wentworth, S.J., Vali, H., Gibson Jr., E.K., Romanek, C.S., 2000. Elongated prismatic magnetite crystals in ALH84001 carbonate globules: potential Martian magnetofossils. Geochimica et Cosmochimica Acta 64, 4049–4081.

Vali, H., Kirschvink, J.L., 1991. Observation of magnetosome organization surface structure and iron biomineralization of undescribed magnetic bacteria: Evolutionary speculations. In: Frankel, R.B., Blakemore, R.P. (Eds.), Iron Biominerals. Springer, Boston, pp. 97–115.

Veevers, J.J., 2004. Gondwanaland from 650–500 Ma assembly through 320 Ma merger in Pangea to 185–100 Ma breakup: supercontinental tectonics via stratigraphy and radiometric dating. Earth-Science Reviews 68, 1–132.

Vesely, F.F., Assine, M.L., 2006. Deglaciation sequences in the Permo-Carboniferous Itararé Group, Paraná Basin, southern Brazil. Journal of South American Earth Sciences 22, 156–168.

von der Heyden, B.P., Roychoudhury, A.N., Mtshali, T.N., Tyliszczak, T., Myneni, S.C.B., 2012. Chemically and geographically distinct solid-phase iron pools in the Southern Ocean. Science 338, 1199–1201.